



Supplement of

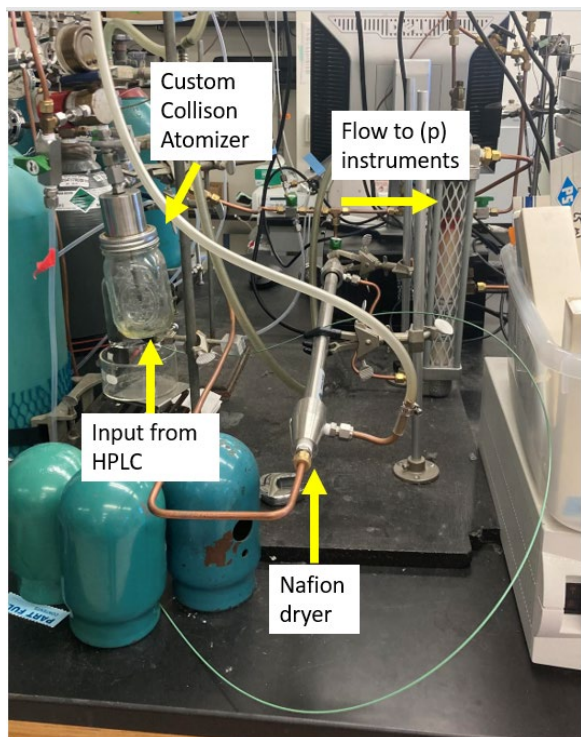
A multi-instrumental approach for calibrating real-time mass spectrometers using high-performance liquid chromatography and positive matrix factorization

Melinda K. Schueneman et al.

Correspondence to: Jose L. Jimenez (jose.jimenez@colorado.edu)

The copyright of individual parts of the supplement might differ from the article licence.

1 **S1 General system information for multi-instrumental calibration method**



2

3 **Figure S1. HPLC tubing into custom atomizer**

4

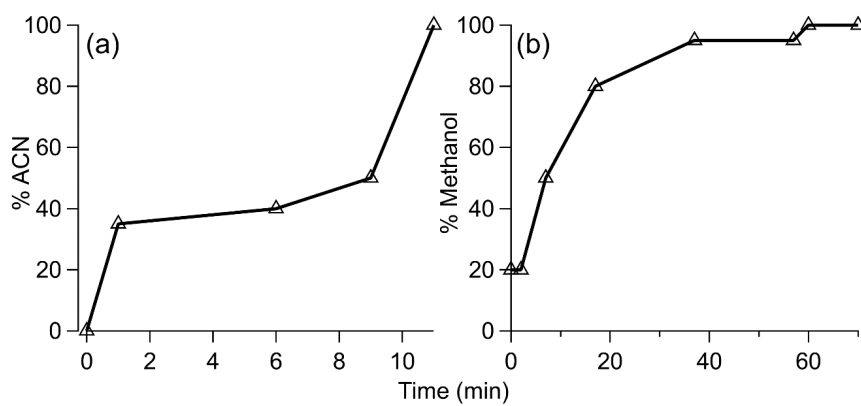
5 **Table S1. Tube volumes, flows, and residence times from HPLC separation to particle instrument detection.**

Item	Total volume (mL)	Flow rate (flow through)	Residence time
Tubing transferring liquid from after HPLC column and UV-Vis detection to atomizer	0.67	1.0 mL min ⁻¹	40 s
Atomizer	500	8.0-10 L min ⁻¹	3.0 - 3.8 s
Nafion drier	7.0	~ 8.0 L min ⁻¹	0.053 s
Tubing before manifold	120	7.2 L min ⁻¹	1.0 s
Post manifold EESI	31	0.84 L min ⁻¹	2.2 s

Post manifold AMS	14	1.5 L min ⁻¹	0.60 s
Post manifold SMPS A	34	1.43 L min ⁻¹	1.4 s
Post manifold SMPS B	29	1.49 L min ⁻¹	1.2 s

6

7



8

9 **Figure S2. Solvent gradients for (a) standard HPLC runs and (b) β -pinene HPLC run. The other solvent was**
 10 **a mixture of 95 % H₂O / 5 % ACN.**

11

12 **Table S2. Standard compounds used for HPLC method demonstration, source and purity, volatility**
 13 **(calculated using published vapor pressures), estimated percent evaporated during transmission (from**
 14 **atomizer output to detection, calculated with C^* and measured OA concentration at detection), and density**
 15 **(using the ratio of d_{va}/d_m)**

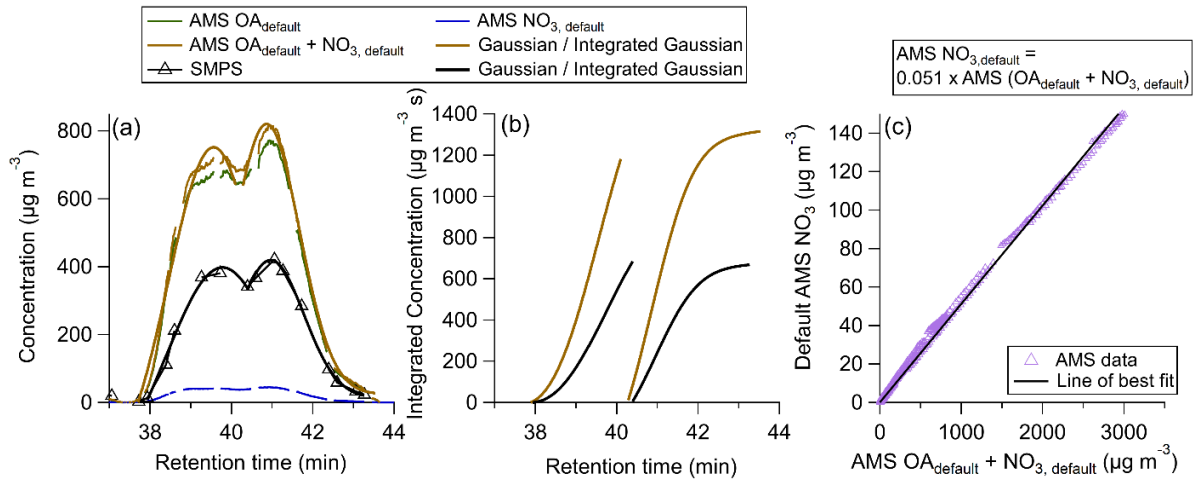
Species	Source + purity	Saturation Mass Concentration ($\mu\text{g m}^{-3}$) (T=298 K)	Estimated Percent Evaporated	Density
3-methyl-4-nitrophenol	Aldrich, 98 %	5,210	92 %	1.27**
Phthalic acid	Beantown Chemical, ACS grade, 99.5 %	5.72	0 %	1.05
4-nitrophenol	Aldrich, 99 %	10,600	94 %	1.48**
Succinic acid	Aldrich, 99 %	1.21	0 %	1.18
4-nitrocatechol	Alfa Aesar, 98 %	64	63 %	1.26
L-malic acid	Aldrich, 97 %	0.24	-	1.28
Citric acid	Fisher Scientific	0.18	-	-
Levoglucosan	Chem-Impex Int'l, \geq 99.0 %	13*	-	1.30
Acetonitrile	Fisher Chemical, > 99.95 %	-	-	-
Methanol	Fisher Chemical, > 99.9 %	-	-	-
Water	VWR Chemicals, HPLC grade	-	-	-
Ethyl Acetate	Fisher Chemical, 99.5 %	-	-	-

16 *Reported in (Pagonis et al., 2021)

17 **Density of bulk solution from literature

18 The densities measured using the d_{va}/d_m ratio do not match the literature values for bulk density well. This is
 19 potentially due to different phases from that of the bulk material, and/or non-spherical particle shape (Jayne et al.,
 20 2000; Huffman et al., 2005). Regardless, the d_{va}/d_m density was used as the best estimate here.

21



22

23 **Figure S3. (a) AMS default mass concentrations for [OA], [NO₃], and [OA + NO₃]; SMPS mass**
 24 **concentrations, corrected for the average density. (b) Integrated Gaussian curves for each peak. (c) Default**
 25 **AMS [NO₃] vs total default AMS signal [OA + NO₃], fit with a line. The slope (ratio of [NO₃] / [OA + NO₃]) =**
 26 **0.051.**

27

28 The nitrate contribution to the total mass for this peak was $\sim 5.1\%$. Fitting the bulk peaks (which are composed of
 29 multiple eluents) may result in some error in the nitrate contribution approximation. CF_x^A was calculated for the two
 30 peaks by referencing the AMS mass to the SMPS mass. For the first peak, $CF_x^A = 1.97$, for the second peak $CF_x^A =$
 31 1.73.

32 S2 SMPS testing and validation

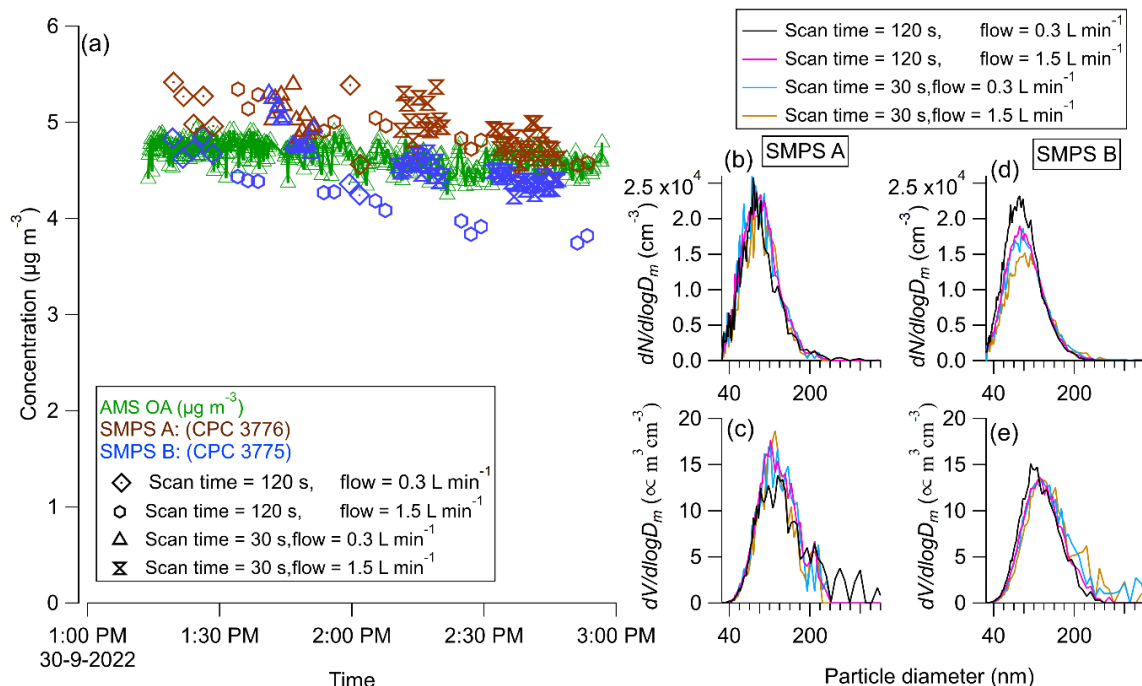
33 S2.1 Fast scanning operation and validation

34 The fast scanning operation of the SMPSs was essential here. A “fast scan” here means 30 s for voltage scanning,
35 with 10 s retrace time (when the voltage is returned back to 0). This allows for an SMPS data point to be obtained
36 every 40 s, and when two SMPSs are used with interleaved timing, every ~ 20 s. This faster scanning is not without
37 precedent; one paper published in 1990 first denoted the term “scanning electrical mobility spectrometer” or SEMS
38 (Wang and Flagan, 1990). In that paper, researchers demonstrated that aerosol distributions for atmospherically
39 relevant samples could be measured in a 30 s scan time, with a 30 s retrace time. This research led to the creation of
40 new SMPSs that, like the SEMS, scanned continuously, and thus would be capable of 30 s scanning times. A study a
41 few years later put this to the test, and looked at the impact of changing SMPS scan times, and found that shorter
42 scan times led to more smearing (less-resolved size distributions) and lower peak maximas (Russell et al., 1995).
43 They suggest that this is driven by the residence time of the particles from the output of the DMA to the optical
44 detection by the CPC (t_d). In addition, a paper in 2002 elaborated on the conclusions from Russell et. al. (1995), and
45 found that when scanning with a flow rate of 0.3 L min^{-1} , combined with a 30 s scan time, the size distribution was
46 significantly broadened (Collins et al., 2002). The maximum concentration was decreased by over 50 % when
47 compared to a longer scan time (300 integrated concentration did not seem as affected, due to broadening in the
48 faster scan.

49 Typically, SMPSs are run at longer scan times of 2 min or more (Sioutas, 1999; McMurry, 2000; Jeong and
50 Evans, 2009). One study modified an SMPS by adding an aerosol particle mass analyzer (APM). With the modified
51 system, data points were recorded every 60 s (Malloy et al., 2009). Another study, which took place on an aircraft
52 and measured the air over Mexico City, ran their SMPS with a scan time of 1.5 min (DeCarlo et al., 2008). Despite
53 the conclusions of Wang and Flagan (1990), many in the community run their SMPSs as “slow” (e.g. scan times of
54 two or more min) instruments. Henceforth, “slow” will refer to the 2 min scans, and “fast” will refer to the 30
55 sscans.

56 Here, we test each SMPS with a combination of “long” scans (2 min scans, 15 s retrace, 3 L min^{-1} sheath
57 flow) and “fast” scans (30 s scans, 10 s retrace, 6 L min^{-1} sheath flow). In order to assess the usability and accuracy
58 of the fast scan method, tests were carried out (Fig. S4) to compare the total integrated volume concentration,
59 number size distributions, and volume size distributions for 2 min scans at both a sample flow of 0.3 L min^{-1} and 1.5
60 L min^{-1} , and 30 s scans done with the same flow rates.

61



62
 63 **Figure S4. (a) Estimated particle mass concentration from SMPS A and B compared to the total OA**
 64 **measured by the AMS, for different combinations of scanning times and sample flow rates when sampling**
 65 **constant DOS concentrations from a large chamber. (b) Number distribution comparisons for different**
 66 **combinations of scanning times and flow rates for SMPS A, (c) Volume distribution comparisons, (d) number**
 67 **distribution comparisons for SMPS B, and (e) volume distribution comparisons for SMPS B.**

68
 69 In Fig. S4a, the total concentration of dioctyl sebacate (DOS) was measured by an AMS (green) and time averaged
 70 to 10 s. The AMS measured DOS (after AMS calibration for that species) was used as the reference concentration.
 71 DOS was generated using a custom evaporation-condensation apparatus (Sinclair and La Mer, 1949; Krechmer et
 72 al., 2017), and flowed into a 20 m³ Teflon chamber. To start, we scanned with both SMPSs set to a 2 min scan time
 73 with a 15 s retrace time, and a flow rate of 0.3 L min⁻¹. This is typically how we run our SMPSs for laboratory
 74 studies and we have compared with even longer scans (up to 300 s, same flow settings) showing good agreement
 75 (Liu et al., 2019) and has shown good quantitative agreement for intercomparisons during chamber and field
 76 campaigns. Those “long scans” serve as a reference. Both SMPSs were run concurrently.

77 Some researchers show peak smearing when using faster scan times (although, those studies seem to use a
 78 sample flow rate=0.3 L min⁻¹) (Russell et al., 1995). These studies posit that the smearing is mainly due to
 79 instrument specific/plumbing delay times from the output of the DMA to the optical detection by the CPC (Russell
 80 et al., 1995). In Fig. S4b, the number distribution is shown for the different flow / scan time configurations for the
 81 SMPS A. The black distribution for all scans is the reference (120 s scan, 0.3L min⁻¹, resolution=10). For the

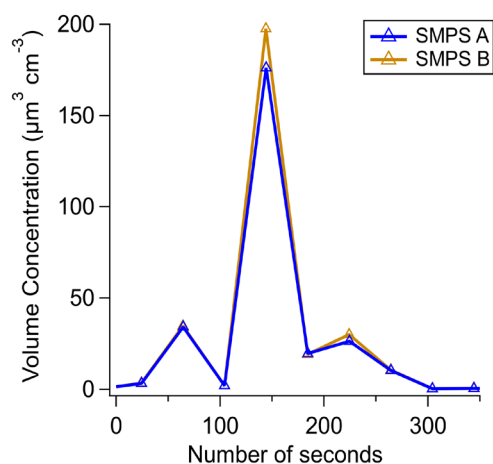
82 number distribution, the peak width for the reference is more narrow than for all other configurations. The difference
83 is minor, however, and not as large as in other reports.

84 In Fig. S4c, the volume distributions are compared. The reference scan has a lower maximum concentration
85 than the other configurations, which seems to go against previously published results. Over time, [DOS] measured
86 by the AMS decreases, due to chamber wall loss effects. To counter this, reference scans (120 scans, 0.3 L min^{-1}
87 flows) are carried out throughout the experiment. For reference, the SMPSs were run with 30 s scans and 1.5 L min^{-1}
88 sample flows for the HPLC method proposed in the main text.

89 The distributions for SMPS B are more affected by the different configurations. This is unsurprising, as it
90 has a longer t_d than SMPS A (table S3), and likely is more representative of the systems studied in the research cited
91 above. In Fig. S4d, the number distribution for the reference scan has a higher maximum than the other scans. The
92 faster, high flow scan is the most different from the reference, and has both a lower maxima and a wider peak width
93 (resolution = 4). This matches previous findings (Collins et al., 2002), but this study shows a far less dramatic peak
94 shape difference than that shown therein. This finding could introduce some quantification error. In Fig. S4, the
95 volume distributions match fairly well for all configurations. A faster instrument (such as an optical particle counter)
96 would be ideal to obtain faster measurements, but the small diameter particles produced by the Collison atomizer
97 makes running those instruments impractical and prone to error (due to low detection efficiency at smaller size
98 particles).

99 For the multi-instrumental calibration experiments, SMPS A and SMPS B were offset by 20 s. That
100 allowed us to obtain a volume concentration every approx. 20 s. For comparing the response between the two
101 SMPSs, an experiment was done where SMPS A and SMPS B were run concurrently (Fig. S5). SMPS A and SMPS
102 B are shown to match within $\sim 0\% - 10\%$ (at the maxima). The consistency observed in Fig. S5 between SMPS A
103 and SMPS B provides increased confidence in the use of each instrument in “fast” mode.

104



105

106 **Figure S5. Concurrent SMPS scans for an HPLC run**

107 **S2.2 SMPS delay time calculations**

108 Delay times from the aerosol sampling manifold to the DMAs were calculated by running each DMA to size select
109 particles with a mobility diameter of 115 nm. Following transmission, the time it takes for the CPC concentration to
110 reach half of its maximum concentration ($t_{1/2}$) was calculated (table S3). Here, delay times were short, due to the
111 high sample flow. This does not eliminate the importance of having accurate delay times. Fast scans are often prone
112 to more error than their slow counterparts.

113 To calculate t_d (table S3), polystyrene latex spheres (PSLs) of a known diameter were atomized and
114 measured by the SMPSs. Calculating delay times ($t_{1/2}$ and t_d [delay time from exit of the DMA to the CPC]) allowed
115 us to properly align the slower SMPS measurements with the fast mass spectrometer measurements during the
116 relatively short chromatographically-separated compound peaks. Each eluting HPLC peak is only approx. 1.5 min
117 long, and the instruments are run at different time resolutions. Each SMPS collects one data point every 40 s. For
118 each data point, the SMPS software provided an uncorrected scanning start time. During the 40 s scan,
119 concentrations can change significantly. If the SMPS scan starts 15 s before the maxima is reached, then the scan is
120 recording concentrations at particle diameters both before, during, and after the peak maxima. If the SMPSs were
121 not corrected for their delay times, then the SMPS data point would show an erroneously low / high concentration,
122 and lead to errors when comparing to the other instruments.

123 **Table S3. Delay times for each SMPS. $t_{1/2}$ is the time it takes for the CPC concentration to reach half of its**
124 **maximum concentration**

SMPS name	CPC type	Delay time ($t_{1/2}$) (s)	DMA to CPC delay time (t_d) (s)
SMPS A	3776	10.5	0.43
SMPS B	3775	8	1.55

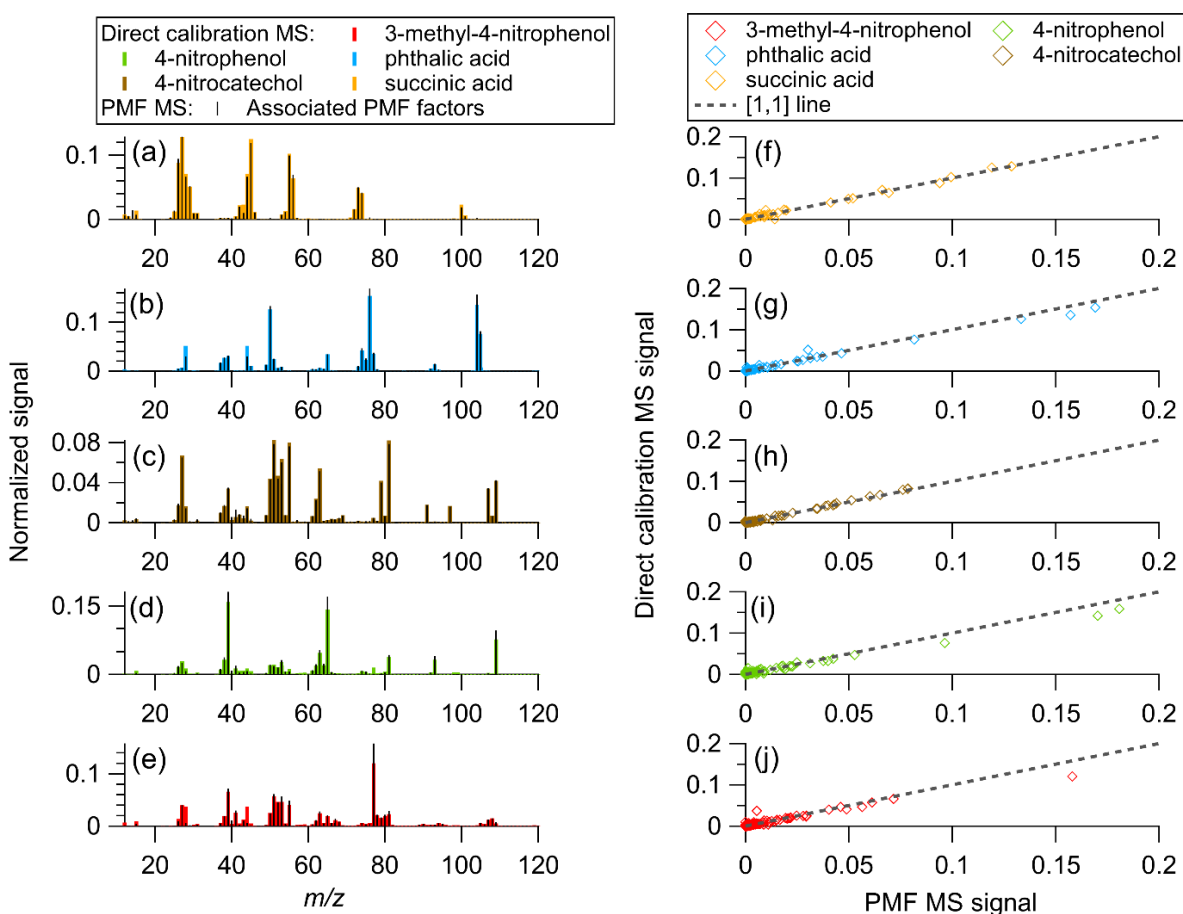
125

126 **S3 Standard mixture mass spectra comparison for direct and multi-instrumental calibrations factors**

127 Mass spectra were obtained from PMF for many of the standards used in Sect. 3.2 and compared against the average
128 mass spectra from direct calibrations (Fig. S6).

129

130



131

132 **Figure S6. (Aa) - (e) Mass spectra for monodisperse calibrations and associated PMF factors for species**
133 **directly calibrated. (f)-(j) scatter plot of MS signal at each measured m/z for the direct calibrations vs the**
134 **PMF mass spectra.**

135

136 The uncentered correlation coefficients (table S4) match well between the assigned PMF factor mass spectra and the
137 corresponding direct calibration mass spectra.

138

139 **Table S4. Uncentered correlation coefficient (UC) between AMS direct calibration and PMF factor mass**
 140 **spectra (Ulbrich et al., 2009)**

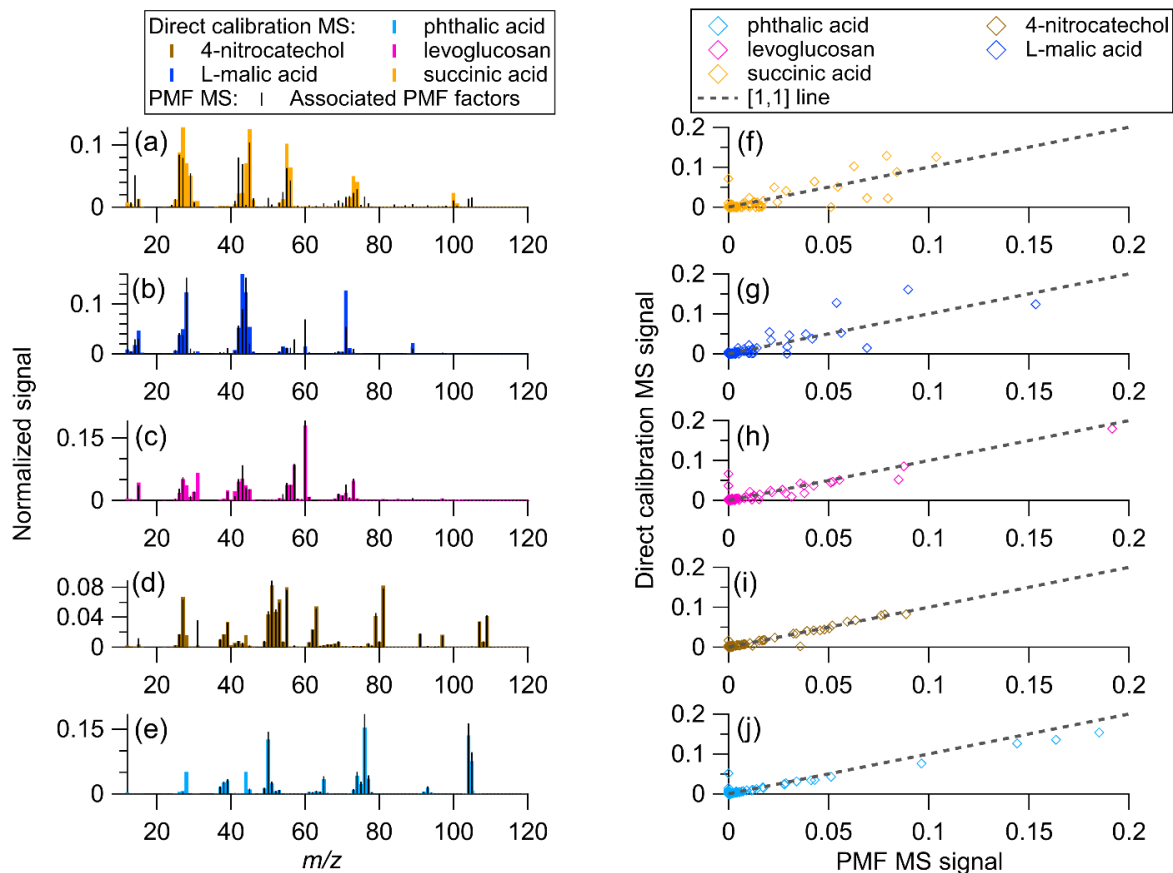
	Direct calibration MS				
PMF factor MS	Succinic acid	4-nitrocatechol	Phthalic acid	4-nitrophenol	3-methyl-4-nitrophenol
Succinic acid	0.99	0.38	0.14	0.15	0.30
4-nitrocatechol	0.38	1.0	0.23	0.49	0.62
Phthalic acid	0.094	0.20	0.99	0.24	0.31
5-nitrophenol	0.10	0.43	0.24	0.99	0.45
3-methyl-4-nitrophenol	0.21	0.58	0.27	0.49	0.96

141

142 The UC provides the same information as the dot product, without the need to normalize the mass spectra. For all
 143 species, the UC > 0.95. For 4-nitrocatechol, the UC rounded up to 1.0 (near perfect agreement).

144 Similarly to the process carried out above, the mass spectra from the PMF solution for the data shown in
 145 Fig. 6 was compared to direct calibrations (Fig. S7).

146



147

148 **Figure S7. (a) - (e) Mass spectra for monodisperse calibrations and associated PMF factors for species**
 149 **directly calibrated for the second standard solution (Fig. 6). (f) - (j) scatter plot of MS signal at each measured**
 150 ***m/z* for the direct calibrations vs the PMF mass spectra.**

151

152 Uncentered correlation coefficients were also calculated (table S5) and generally showed less agreement than those
 153 shown in table S4.

154 **Table S5. Uncentered correlation coefficient (UC) between AMS direct calibration and PMF factor mass**
 155 **spectra (Ulbrich et al., 2009) for standard solution 2 (Fig. 6, Fig. S7)**

	Direct calibration MS				
PMF factor MS	Succinic acid	L-malic acid	Levogluconan	4-nitrocatechol	Phthalic acid
Succinic acid	0.81	0.50	0.35	0.31	0.17
L-malic acid	0.55	0.89	0.60	0.20	0.23
Levogluconan	0.36	0.41	0.93	0.19	0.029
4-nitrocatechol	0.33	0.12	0.23	0.98	0.20
Phthalic acid	0.030	0.014	0.025	0.19	0.96

156

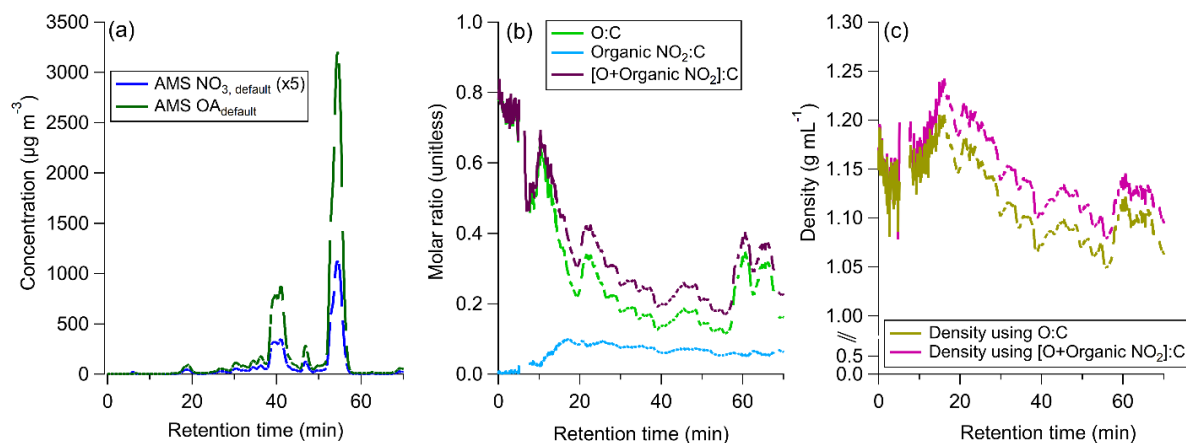
157 Levogluconan, 4-nitrocatechol, and phthalic acid match well (UC > 0.9). Succinic acid and L-malic acid match less
 158 well, but still have a UC > 0.8. As expected, the UC's for the second standard solution are less good than those for
 159 the first standard solution (which was almost entirely resolved even without PMF).

160 **S4 β -pinene detailed information: density, molecular identification, PMF solution, and peak fitting**

161 For the SOA samples, the effective density was calculated as described in Sect. 2.5.2, shown in Fig. S8.

162

163

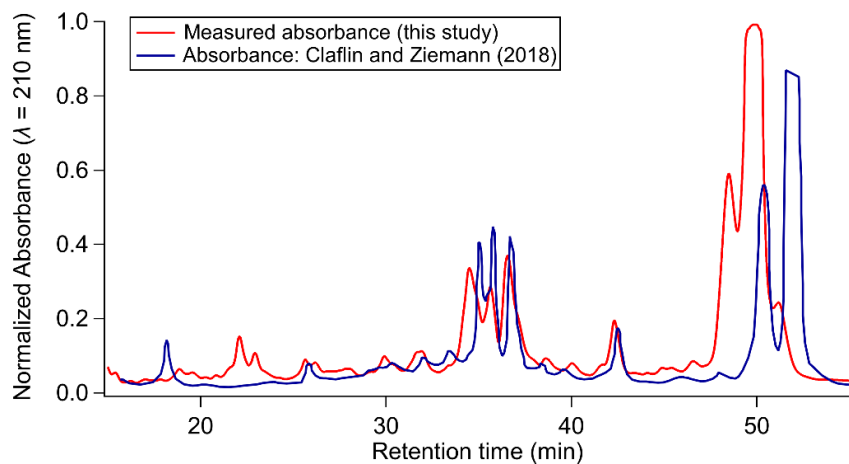


164 **Figure S8. (a) Measured NO_3 and OA from the AMS when sampling β -pinene + NO_3 SOA. (b) Atomic ratios**
165 **for organic nitrate : carbon, oxygen to carbon, and oxygen + organonitrates to carbon. (c) Estimated density**
166 **from two approaches.**

168

169 The chromatogram from Claflin and Ziemann (2018) was compared to that measured here (Fig. 7), shown below in
170 Fig. S9.

171



172

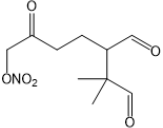
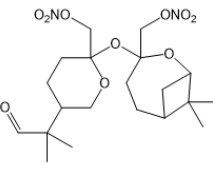
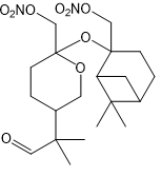
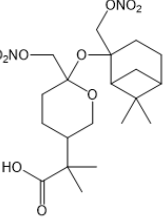
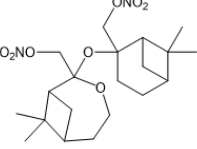
173 **Figure S9. Comparison to β -pinene + NO_3 SOA chromatogram measured in Claflin and Ziemann (2018).**

174

175 The chromatograms show the same general shape, although with slightly faster elution for this work. There are some
 176 notable differences in the results between 20 - 30 min and 45 - 55 min. The final peak in the chromatogram from
 177 Claflin and Ziemann is the same peak as the largest one measured here (retention time ~ 50 min). This suggests that
 178 there could be some difference in the HPLC gradient method, or a potential contamination in one of the HPLC
 179 solvents. Despite that, the overall signals are consistent, and some of the identified species are shown in table S6.

180

181 **Table S6. Structure of some known species (from Claflin and Ziemann (2018)), exact (theoretical) mass,**
 182 **observed mass (measured with EESI+), and mass accuracy (based on EESI instrument multiion m/z**
 183 **calibration fit).**

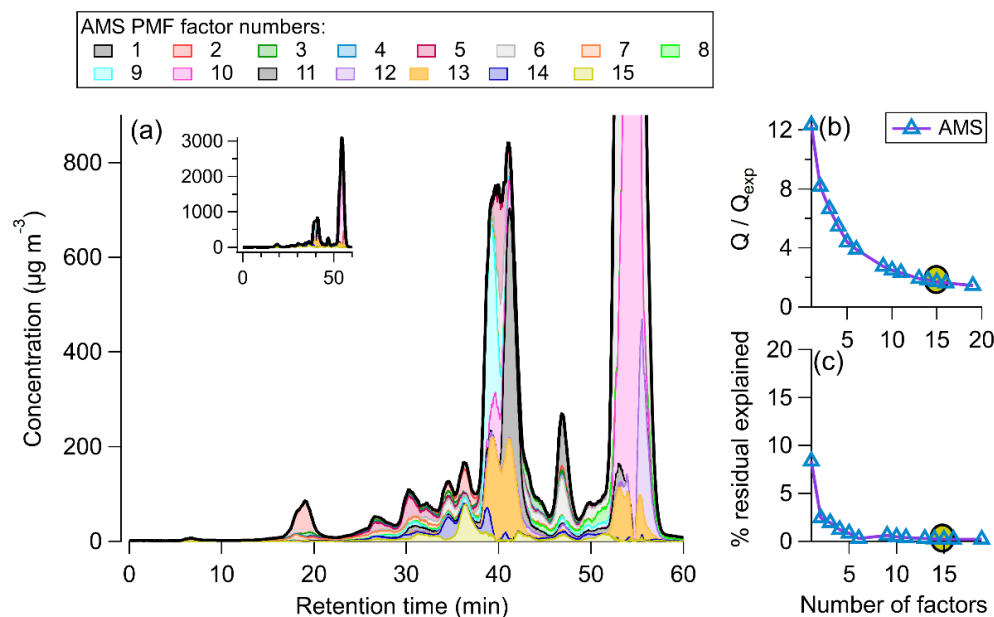
Structure					
MW	245.23	460.48	444.48	460.48	428.48
Exact mass (+Na ⁺) (Da)	268.0797	483.1955	467.2002	483.1955	451.2056
Detected mass (Da)	268.0879	483.1885	467.2032	483.1885	451.2120
Mass Accuracy (ppm)	30.6	-14.5	6.42	-14.5	14.2

184

185

186 PMF was run on the AMS data, shown below for the entire HPLC run (Fig. S10).

187



188
 189 **Figure S10. (a) stacked plot showing AMS PMF solution time series for the β -pinene + NO_3 SOA system, with**
 190 **inset showing full scale. (b) Q / Q_{expected} , with the chosen solution (15 factors) circled. (c) Percent of the total**
 191 **sum of the residuals explained, 15 factor solution circled.**

192
 193 A 15 factor solution was chosen. The time series and mass spectra for each factor are shown in Fig. S11. The AMS
 194 signal during the β -pinene + NO_3 HPLC experiment was high, ranging from $\sim 100 - 4000 \mu\text{g m}^{-3}$. For low volatility
 195 species, these high concentrations are not necessary. However, in many systems, the volatility of the produced
 196 products will range many orders of magnitude in C^* . To best calibrate for low-volatility and semi-volatile products,
 197 higher concentrations of SOA should be injected into the column. For the β -pinene+ NO_3 SOA that was shown here,
 198 the chamber experiment (as discussed in Clafin and Ziemann, 2018), started with the addition of $\sim 200 \mu\text{g m}^{-3}$
 199 ammonium sulfate seed, 1 ppm of β -pinene, and 0.3 ppm N_2O_5 (in an 8.0 m^3 Teflon FEP chamber). All of the N_2O_5
 200 was reacted, meaning ~ 0.3 ppm of β -pinene was reacted. The amount of SOA formed can be calculated using the
 201 known SOA yields, concentrations, and flow rates.

202 First, 0.3 ppm β -pinene is converted into a mass concentration. Following this step, the mass concentration
 203 is multiplied by the known SOA yield (Eq. S1)

$$204 \quad \text{SOA yield} = \frac{\Delta\text{SOA}}{\Delta\text{VOC}} \quad \text{Eq. S1}$$

205 The SOA yield for this system ranges from $\sim 27 - \sim 105 \%$ (Boyd et al. 2015). If 30 % of the β -pinene reacted, then
 206 the amount of SOA was formed ranged from $372 \mu\text{g m}^{-3}$ to $1378 \mu\text{g m}^{-3}$. This concentration of aerosol was then
 207 collected on a filter at a flow rate of 14 L min^{-1} for 120 min. This would imply that $625 \mu\text{g} - 2315 \mu\text{g}$ of SOA was
 208 collected on the filter. Assuming a 100 % extraction efficiency of SOA, the amount of material injected into the
 209 column can be quantified as such (Eq. S2)

210
$$\text{Injected mass} = \frac{\text{mass SOA}}{\text{volume ACN}} \times \text{injected volume of solution} \quad \text{Eq. S2}$$

211 A typical volume of acetonitrile (ACN) used would be ~ 2 mL, therefore the concentration of SOA in ACN would
212 range from $313 \mu\text{g mL}^{-1}$ - $1158 \mu\text{g mL}^{-1}$. The maximum injected volume is $50 \mu\text{L}$, therefore the total injected mass
213 ranges from $16 \mu\text{g}$ - $58 \mu\text{g}$.

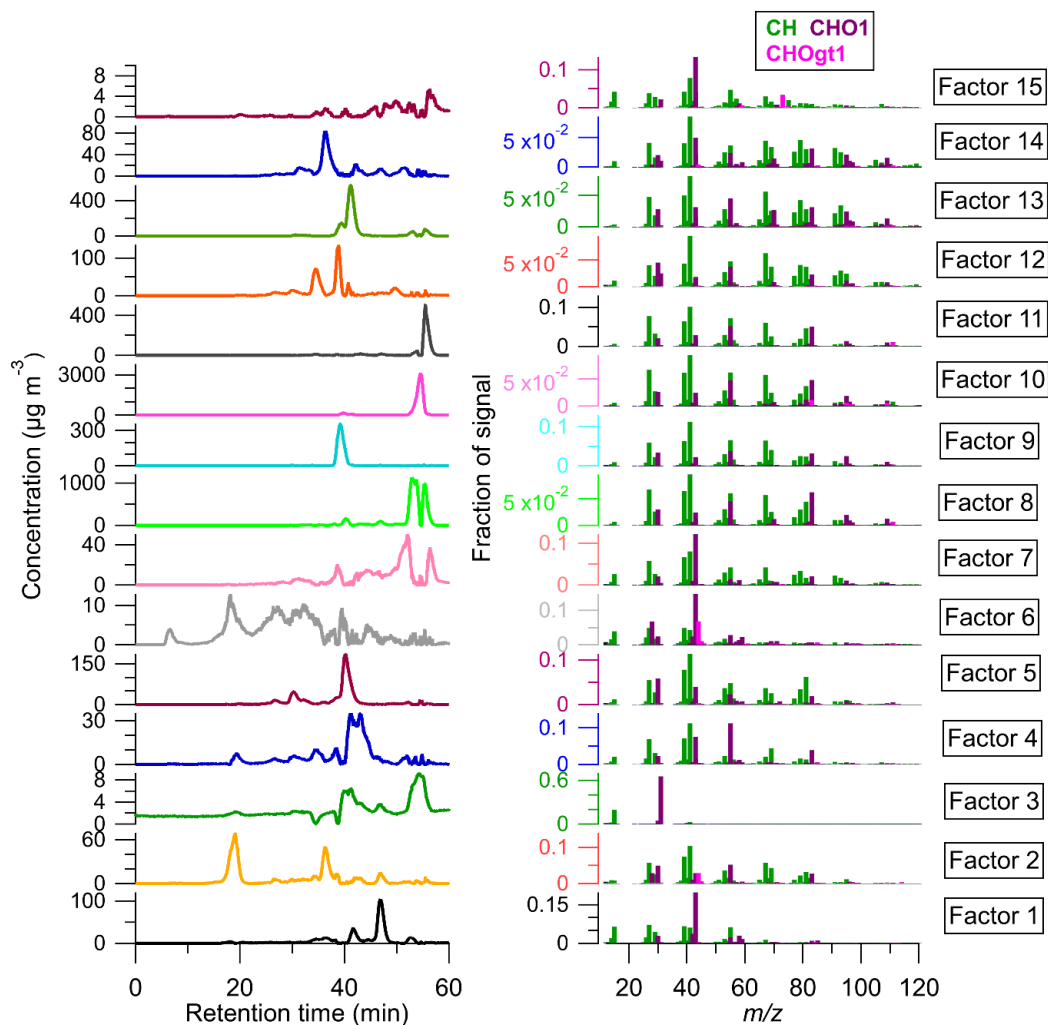
214 To confirm these results, we use the largest peak in the chromatogram (m/z 451.2, retention time ~ 55 min)
215 in an example. According to Clafin and Ziemann (2018), this peak is responsible for ~ 55 % of the total SOA in this
216 system. Therefore, anywhere from $8.8 \mu\text{g}$ - $32 \mu\text{g}$ of the injected mass comes from that peak. However, only 0.55 %
217 of that mass makes it to the instruments, so the instruments should observe 0.048 - $0.18 \mu\text{g}$.

218 The observed AMS mass concentration was roughly $2000 \mu\text{g m}^{-3}$ using the corrected CF_x^A . If we assume the peak is
219 a triangle, we can estimate the area by multiplying the observed peak mass concentration by the total peak elution
220 time (~ 2 min on average) and dividing by 2. This value is $2000 \mu\text{g m}^{-3} \times \text{min}$. The AMS flow was $\sim 0.1 \text{ L min}^{-1}$ or
221 $1 \times 10^{-4} \text{ m}^3 \text{ min}$, so the AMS sampled $\sim 0.2 \mu\text{g}$, which is very close to the $0.18 \mu\text{g}$ estimated above.

222 These injected solution concentrations were able to produce the AMS concentrations observed in Fig. 7,
223 Fig. S8, Fig. S10, and Fig. S12. For species with a volatility (C^*) $> 100 \mu\text{g m}^{-3}$, there would be substantial
224 evaporation, > 50 % at equilibrium. While some evaporation would occur for species with a volatility $< 100 \mu\text{g m}^{-3}$,
225 like 4-nitrocatechol in Fig. 4, the SMPS, AMS, and EESI seem to mostly agree.

226 It should be noted that, in our setup, < 1 % of the injected mass made it to the mass spectrometers. The use
227 of the collected sample could be optimized further, allowing the analysis of smaller amounts of mass by this method.

228



229

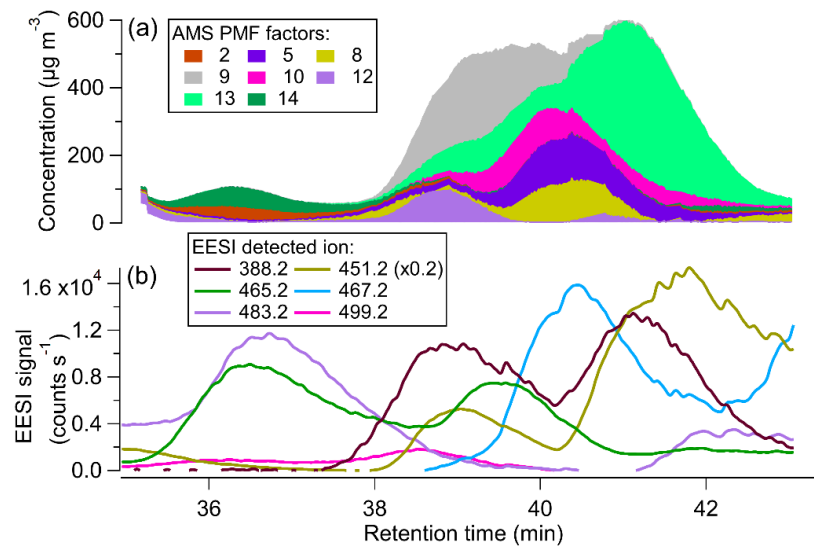
230 **Figure S11. (Left) time series of individual PMF factors for the β -pinene + NO₃ SOA system and (right) HR**
 231 **mass spectra (colored by family) for each factor.**

232

233 Many of the factors have different time series but very similar mass spectra. This suggests that the species fragment
 234 similarly in the AMS (and likely have similar phase states). The SOA products are mostly hydrocarbons with polar
 235 moieties (nitrate, carboxylic acids, ketones, and cyclic ethers). Many of the species retained the nonpolar moiety
 236 from injection to detection (as shown in the CH dominated mass spectra).

237 The peaks eluting from ~ 35 - ~ 43 min showed the strongest overlap (and also contained many of the
 238 known β -pinene + NO₃ SOA products). The time series for this portion of the HPLC run is shown in Fig. S12.

239



240
 241 **Figure S12. (a) stacked plot of AMS PMF factors from 35 - 43 min and (b) EESI HR ions time series.**

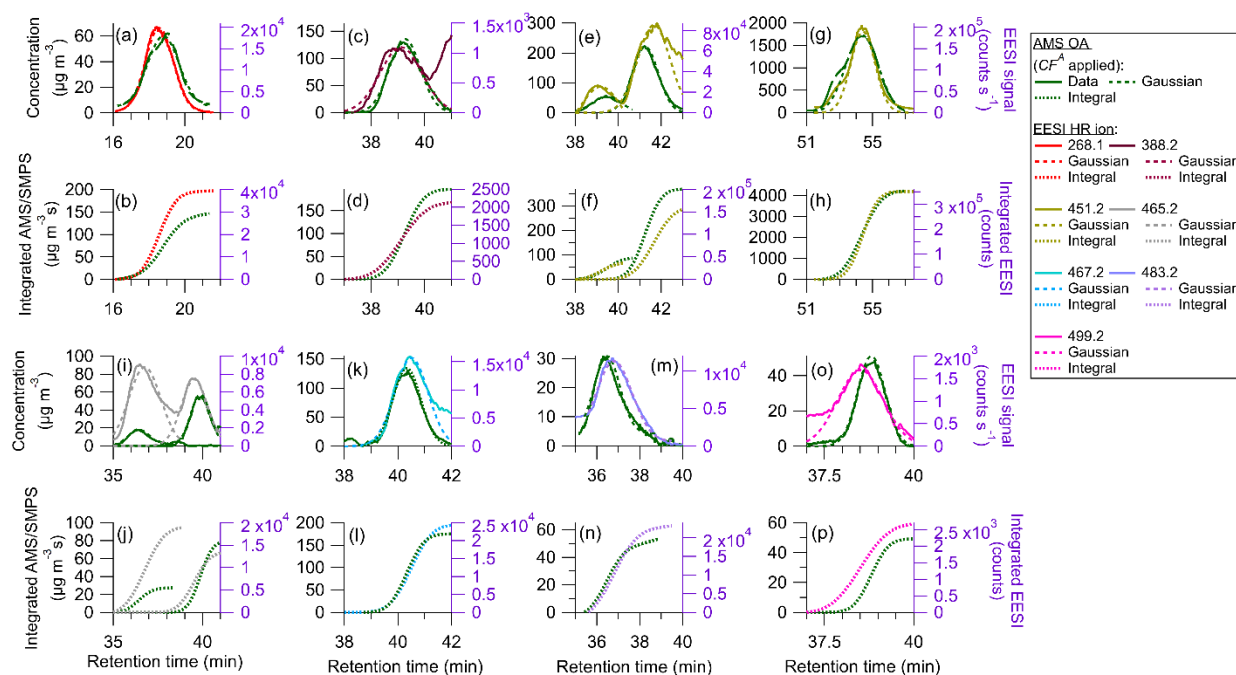
242
 243 As described in Sect. 3.3, EESI HR ions were matched to AMS PMF factors using the shape of the time series' as
 244 well as the retention times. The EESI HR ions and associated AMS PMF factors are shown in Table S7.

245 **Table S7. EESI HR ion and corresponding AMS PMF factor(s)**

EESI HR ion	Associated AMS PMF factor(s)
268.1	-
388.2	9, 13
451.2 (1)	13
451.2 (2)	13
451.2 (3)	-
465.2 (1)	2
465.2 (2)	10
467.2	5,8
483.2	14

246
 247 Individual peaks are shown in Fig. S13.

248



250
 251 **Figure S13. (a) m/z 268.1 Gaussians, (b) integrals; (c) m/z 388.2 Gaussians, (d) integrals; (e) one peak for m/z**
 252 **451.2 Gaussians, (f) integrals; (g) one peak for m/z 451.2 Gaussians, (h) integrals; (i) m/z 465.2 Gaussians, (j)**
 253 **integrals; (k) m/z 467.2 Gaussians, (l) integrals; (m) one peak for m/z 483.2 Gaussians, (n) integrals; (o) m/z**
 254 **499.2 Gaussians, (p) integrals. For the EESI HR ions, the total mass (OA + NO₃) was used in the**
 255 **denominator.**

256 Not every peak observed in Clafin and Ziemann (2018) was identified here, which is likely due to lack of EESI
 257 sensitivity to some species and potential decomposition of SOA products (specifically for the trimer identified in
 258 Clafin and Ziemann (2018)). In contrast, some EESI HR ions that do not correspond to peaks identified in Clafin
 259 and Ziemann (2018) were detected here, but structures for those species are unknown. All identified individual
 260 peaks are shown in Fig. S13. As described in Sect. 2.7, CF_x^E was determined either using the measured SMPS mass
 261 or the total AMS mass (OA + NO₃). Fig. S13 shows the AMS OA mass, which was separated by PMF. As shown in
 262 Fig. S3, the NO₃ contribution to the total mass was ~ 5 %. This contribution was added to the denominator to
 263 calculate CF_x^E which are reported in table 2 in the main text.

264 **References**

- 265 Boyd, C. M., J. Sanchez, L. Xu, a. J. Eugene, T. Nah, W. Y. Tuet, M. I. Guzman, and N. L. Ng. 2015. “Secondary
266 Organic Aerosol Formation from the β -Pinene+NO₃ System: Effect of Humidity and Peroxy Radical Fate.”
267 *Atmospheric Chemistry and Physics* 15 (13): 7497–7522.
268
- 269 Clafflin, M. S. and Ziemann, P. J.: Identification and Quantitation of Aerosol Products of the Reaction of β -Pinene
270 with NO₃ Radicals and Implications for Gas- and Particle-Phase Reaction Mechanisms, *J. Phys. Chem. A*, 122(14),
271 3640–3652, doi:10.1021/acs.jpca.8b00692, 2018.
272 Collins, D. R., Flagan, R. C. and Seinfeld, J. H.: Improved inversion of scanning DMA data, *Aerosol Sci. Technol.*,
273 36(1), 1–9, doi:10.1080/027868202753339032, 2002.
- 274 DeCarlo, P. F., Dunlea, E. J., Kimmel, J. R., Aiken, A. C., Sueper, D., Crouse, J., Wennberg, P. O., Emmons, L.,
275 Shinozuka, Y., Clarke, A. and Others: Fast airborne aerosol size and chemistry measurements above Mexico City
276 and Central Mexico during the MILAGRO campaign, 1foldr Import 2019-10-08 Batch 1 [online] Available from:
277 <https://oaktrust.library.tamu.edu/bitstream/handle/1969.1/178622/document-2.pdf?sequence=2>, 2008.
- 278 Huffman, J. A., Jayne, J. T., Drewnick, F., Aiken, A. C., Onasch, T., Worsnop, D. R. and Jimenez, J. L.: Design,
279 Modeling, Optimization, and Experimental Tests of a Particle Beam Width Probe for the Aerodyne Aerosol Mass
280 Spectrometer, *Aerosol Sci. Technol.*, 39(12), 1143–1163, doi:10.1080/02786820500423782, 2005.
- 281 Jayne, J. T., Leard, D. C., Zhang, X., Davidovits, P., Smith, K. A., Kolb, C. E. and Worsnop, D. R.: Development of
282 an Aerosol Mass Spectrometer for Size and Composition Analysis of Submicron Particles, *Aerosol Sci. Technol.*,
283 33(1-2), 49–70, doi:10.1080/027868200410840, 2000.
- 284 Jeong, C.-H. and Evans, G. J.: Inter-Comparison of a Fast Mobility Particle Sizer and a Scanning Mobility Particle
285 Sizer Incorporating an Ultrafine Water-Based Condensation Particle Counter, *Aerosol Sci. Technol.*, 43(4), 364–
286 373, doi:10.1080/02786820802662939, 2009.
- 287 Krechmer, J. E., Day, D. A., Ziemann, P. J. and Jimenez, J. L.: Direct Measurements of Gas/Particle Partitioning
288 and Mass Accommodation Coefficients in Environmental Chambers, *Environ. Sci. Technol.*, 51(20), 11867–11875,
289 doi:10.1021/acs.est.7b02144, 2017.
- 290 Malloy, Q. G. J., Nakao, S., Qi, L., Austin, R., Stothers, C., Hagino, H. and Cocker, D. R.: Real-Time Aerosol
291 Density Determination Utilizing a Modified Scanning Mobility Particle Sizer—Aerosol Particle Mass Analyzer
292 System, *Aerosol Sci. Technol.*, 43(7), 673–678, doi:10.1080/02786820902832960, 2009.
- 293 McMurry, P. H.: A review of atmospheric aerosol measurements, *Atmos. Environ.*, 34(12), 1959–1999,
294 doi:10.1016/S1352-2310(99)00455-0, 2000.
- 295 Pagonis, D., Campuzano-Jost, P., Guo, H., Day, D. A., Schueneman, M. K., Brown, W. L., Nault, B. A., Stark, H.,
296 Siemens, K., Laskin, A., Piel, F., Tomsche, L., Wisthaler, A., Coggon, M. M., Gkatzelis, G. I., Halliday, H. S.,
297 Krechmer, J. E., Moore, R. H., Thomson, D. S., Warneke, C., Wiggins, E. B. and Jimenez, J. L.: Airborne extractive
298 electrospray mass spectrometry measurements of the chemical composition of organic aerosol, *Atmospheric*
299 *Measurement Techniques*, 14(2), 1545–1559, doi:10.5194/amt-14-1545-2021, 2021.
- 300 Russell, L. M., Flagan, R. C. and Seinfeld, J. H.: Asymmetric Instrument Response Resulting from Mixing Effects
301 in Accelerated DMA-CPC Measurements, *Aerosol Sci. Technol.*, 23(4), 491–509,
302 doi:10.1080/02786829508965332, 1995.
- 303 Sinclair, D. and La Mer, V. K.: Light scattering as a measure of particle size in aerosols; the production of
304 monodisperse aerosols, *Chem. Rev.*, 44(2), 245–267, doi:10.1021/cr60138a001, 1949.
- 305 Sioutas, C.: Evaluation of the Measurement Performance of the Scanning Mobility Particle Sizer and Aerodynamic
306 Particle Sizer, *Aerosol Sci. Technol.*, 30(1), 84–92, doi:10.1080/027868299304903, 1999.

- 307 Ulbrich, I. M., Canagaratna, M. R., Zhang, Q., Worsnop, D. R. and Jimenez, J. L.: Interpretation of organic
308 components from positive matrix factorization of aerosol mass spectrometric data, *Atmospheric Chemistry &*
309 *Physics*, 9(9) [online] Available from: <https://d-nb.info/114970523X/34>, 2009.
- 310 Wang, S. C. and Flagan, R. C.: Scanning Electrical Mobility Spectrometer, *Aerosol Sci. Technol.*, 13(2), 230–240,
311 doi:10.1080/02786829008959441, 1990.